The Effective Temperatures of O-type Stars from UV spectroscopy

Luciana Bianchi[a], Miriam Garcia[b]

[a]*Johns Hopkins University, Baltimore, USA*
[b]*Center for Astrobiology, INTA-CSIC, Torrejon de Ardoz, Spain*

Abstract

We present an analysis of high resolution spectra in the far-UV $-$ UV range ($\sim$905-2000Å) with non-LTE, spherical, hydrodynamical, line-blanketed models, of three O-type Galactic stars, and derive their photospheric and wind parameters. These data extend previously analyzed samples and fill a gap in spectral type coverage. The combined sample confirms a revised (downward) T_{eff} scale with respect to canonical calibrations, as found in our previous works from UV and optical spectra, and in recent works by other authors.

Keywords: Stars: fundamental parameters, stars: mass loss, stars: early-type, stars: winds, outflows, ultraviolet: stars

1. Introduction

Massive stars play a crucial role in the chemical and dynamical evolution of stellar structures in the Universe, for their feedback of energy and chemically-enriched material to the interstellar medium. Accurate estimates of the physical parameters of massive stars are relevant for understanding their evolution, and ultimately the chemical evolution of galaxies. Yet outstanding questions remain to be answered concerning these objects; for O-type stars, among the most massive stellar objects, there is still lack of consensus on their stellar parameters, such as the effective temperature (T_{eff}) and mass-loss rate ($\dot{M}$) in particular.

Email addresses: `bianchi@pha.jhu.edu` (Luciana Bianchi), `mgg@cab.inta-csic.es` (Miriam Garcia)
URL: `http://dolomiti.pha.jhu.edu` (Luciana Bianchi)

In the past decade, significant steps forward were made possible by the *Far Ultraviolet Spectroscopic Explorer* (FUSE), that enabled access to critical diagnostic lines for hot star winds, with spectroscopy in the far-UV ($\Delta\lambda$=905-1187Å) range. At the same time, major progress in calculations of stellar atmospheres with expanding winds contributed to refined analysis of both UV and optical diagnostics. As part of our effort in this field, we had analyzed far-UV (FUSE), UV and optical spectra of hot massive stars in the Galaxy with non-LTE model atmospheres with expanding winds, to estimate photospheric and wind parameters including T_{eff}, L_{bol}, log g , $\dot{M}$, and v_∞(Bianchi & Garcia (2002), Garcia & Bianchi (2004) and Bianchi, Herald & Garcia (2009), hereafter BG02, GB04 and BHG09). Lines of the most abundant ionic species in the expanding winds, including high ionization stages (e.g. OVI) and low-abundance non-CNO elements (e.g. SVI, SIV, PV) in the far-UV, in addition to NIV, NV, CIV and SiIV transitions in the UV range, play a crucial role for uniquely constraining some stellar parameters. Such diagnostics enable us to solve consistently the ionization structure in the stellar wind (e.g., BHG09), and to find a solution for the stellar parameters that reconciles lines of different ionization potential.

The most significant result was that for all stars analysed, including mid-O types (BG02) and earlier types (GB04), the $T_{\rm eff}$ derived from our analysis is significantly lower than previous estimates, and than values attributed to their spectral types by classical compilations. Consequently, the luminosities are also lower.

Downwards revisions of $T_{\rm eff}$ were independently confirmed by analyses of optical spectra of hot massive stars with state of the art models, calculated with FASTWIND (Puls et al., 2005) and CMFGEN (Hillier & Miller, 1998, 1999). Such analyses (e.g. Martins, Schaerer, & Hillier (2005); Herrero, Puls, & Najarro (2002); Repolust, Puls, & Herrero (2004)), also pointed towards lower $T_{\rm eff}$'s than previous works based on pure H and He models, a result qualitatively similar to our findings, although in detail small discrepancies remained among different diagnostics, and modeling treatements. Reconciling UV and optical diagnostics can ultimately be achieved by an adequate treatement of clumping in the wind, as shown e.g. by BHG09 and by Bouret et al. (2012).

Here we present FUSE observations of early and mid-O type stars, and a preliminary analysis combining these data with UV spectra. The paper is arranged as follows: in Section 2 the data reduction is explained; in Section 3 the spectral morphology of the new targets together with the previous

Table 1: Datasets used in this work

Star	*FUSE*	*IUE-SWP*
HD 16691	E8050101	SWP08323, SWP08288
HD 151300	E80505-01,-02,-03,-04	–
HD 152386	E8050601	SWP02848

samples is described; the quantitative analysis of the spectra is presented in Section 4; results are discussed in Section 5.

2. Spectroscopic Data and Reduction

2.1. FUSE far-UV spectra

The FUSE data presented here were obtained as part of program E805 (P.I.: L. Bianchi), aimed at improving the coverage of the FUSE archive for early spectral types; in particular, the lack of high luminosity objects of the earliest types, but also the lack of redundancy. The latter is essential for a meaningful calibration of fundamental stellar parameters, since the far-UV spectrum of the most massive stars may reveal peculiarities not predictable from their optical spectra (e.g. BG02). The program was not completed because of FUSE gyros failure; three targets were observed: HD 16691 (O4 If+, Walborn (1973)), HD 151300 (O5.5 III(f), Garrison, Hiltner, & Schild (1977)) and HD 152386 (O6 Iafpe, Walborn (1973)).

The FUSE data were taken through the *LWRS* aperture ($30'' \times 30''$) in *timetag* mode; they have a resolution of $\lambda/\Delta\lambda \geq 20,000$. We aimed at a signal to noise ratio (S/N) of S/N$\gtrsim$15 per 0.25Å resolution element; one target, HD 151300, was observed for a longer time than planned, therefore the S/N of its spectrum is higher.

The data were reduced with the pipeline CalFUSE (Dixon, Kruk, & Murphy, 2001). All the LiF and SiC segments of every exposure were examined to verify optimal centering of the spectra in the extraction window and to avoid data defects such as event bursts or the "worm" (Sahnow et al., 2000; Sahnow , 2002). To minimize the contamination from airglow lines, only the nighttime photons were used. We ran the pipeline on individual exposures, to verify mirror alignment and to correct for aberrations, then we combined them and subtracted the background. In this increased S/N image a more accurate background subtraction is achieved.
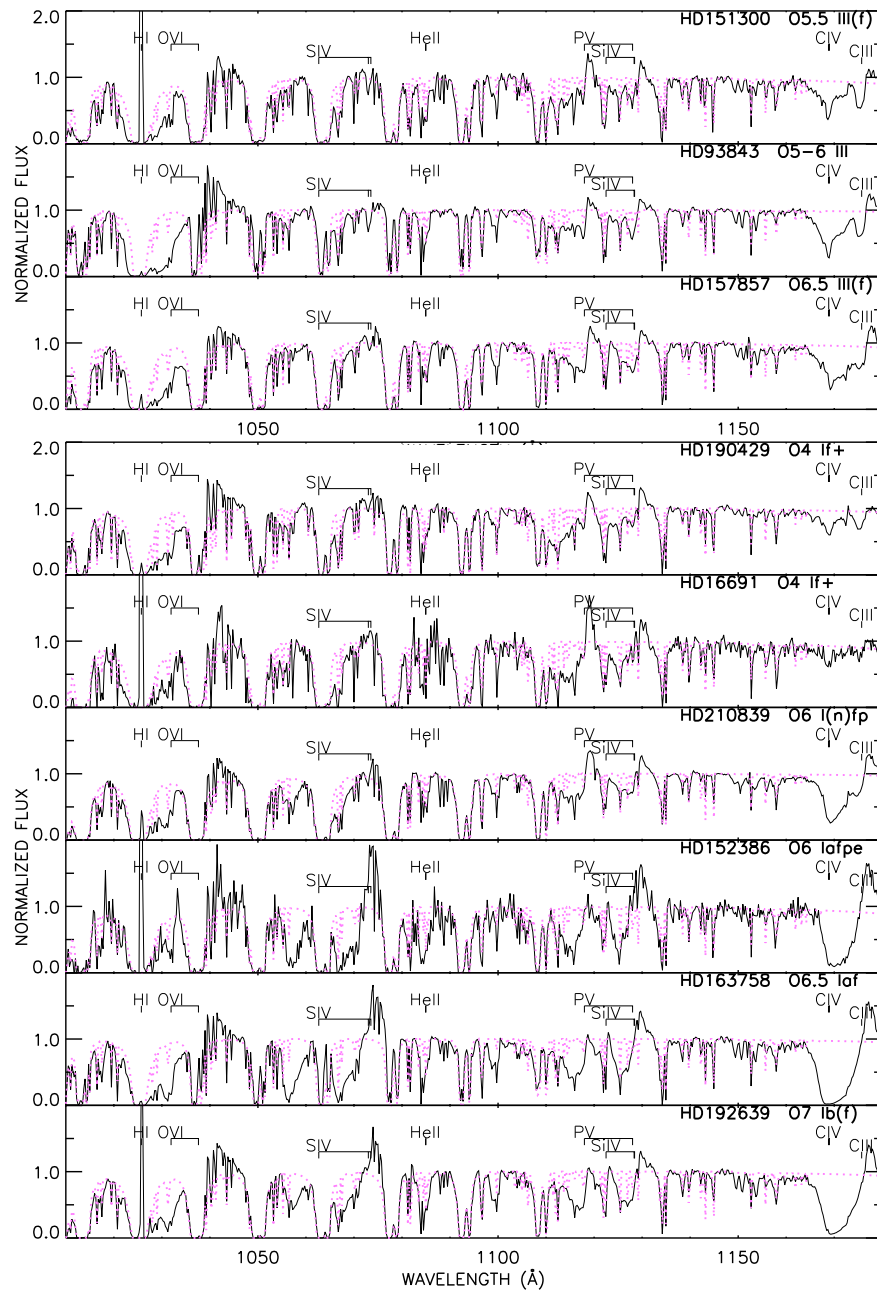
Figure 1: **Bottom:** Far-UV spectra of O-type supergiants. The pink/grey dotted line is the estimated interstellar hydrogen absorption towards each object. The CIV+CIII blend decreases smoothly towards earlier types. PV+SiIV and SIV peak in intensity around type O6 (note, however, that HD 152386 has a "fe" type). **Top:** FUSE spectra of HD151300 compared with the giants analyzed by BG02. All lines except OVI are weaker than in the spectra of the supergiants of similar spectral type. PV+SiIV varies with spectral type as in the supergiants sequence. CIV+CIII decreases towards earlier types.
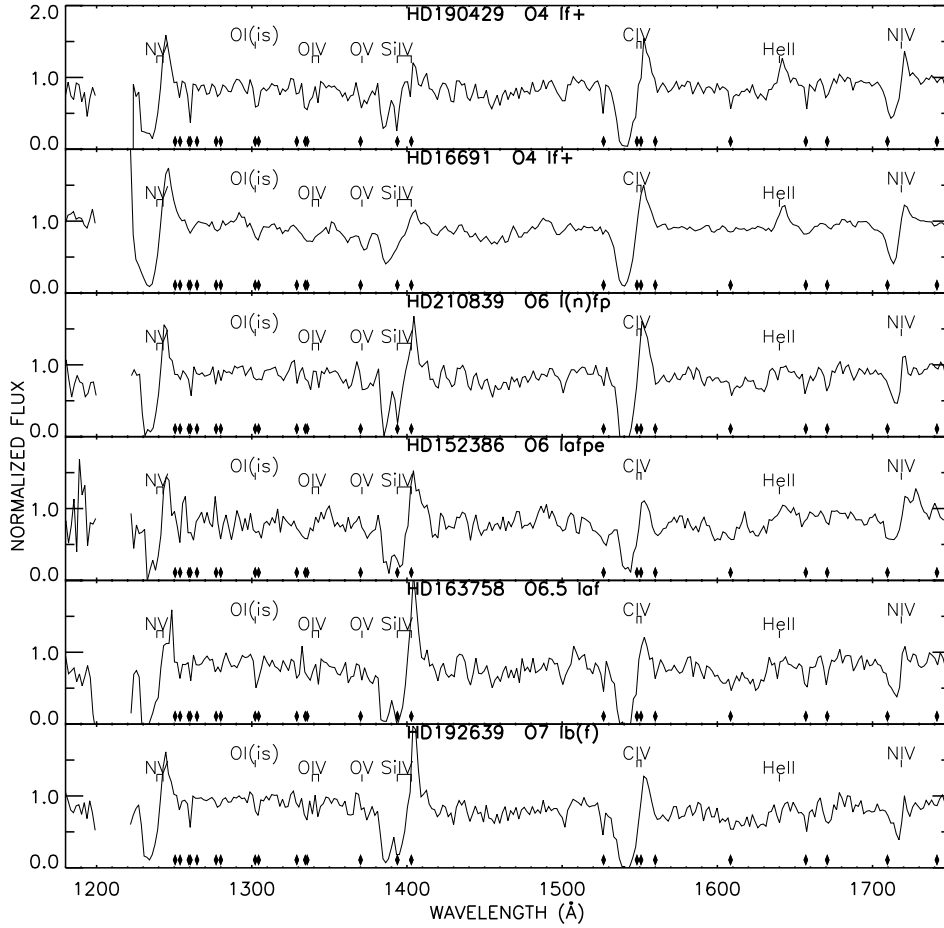
Figure 2: Spectral morphology of O-supergiants in the UV. The diamonds at the bottom of each box mark the most prominent interstellar lines. The strength of SiIV $\lambda\lambda$1393.8,1402.8 decreases from O7 to O4 types. HeII λ1640 displays a prominent emission in the two O4 supergiants.

5

HD 151300 was observed by FUSE during four visits. We compared the spectra taken in each visit, after fully processing them separately, and found no variations of line profiles or continuum flux in visits 2, 3 and 4. Therefore, to improve S/N, we combined all raw exposures taken during these visits (except for the first exposure of visit 4) before applying background subtraction. Visit 1 was not included because it has poorer S/N; we found differences between the flux levels of different segments, and portions of the spectrum have negative fluxes. For the other two targets, all exposures and segments were combined.

The spectra were extracted from the combined exposures and checked with the *IDL* code *fuse_register* (Lindler, 2002) for flux consistency and wavelength alignment among different channels. Then, the good portions from different channels were combined into a final spectrum: SiC2A in the region of $\lambda \lesssim 1000$Å, LiF1A in the 1000Å$\lesssim \lambda \lesssim 1080$Å and LiF2A for $\lambda \gtrsim 1090$Å. For HD 152386 we used LiF2B data in the 1000Å$\lesssim \lambda \lesssim 1080$Å interval because the "1A" segments show negative portions despite the improved background subtraction. The wavelength ranges 905-930Å and 1181-1187Å, at the ends of the *FUSE* range, have poor quality and were not used in this work. The 1082.5-1087Å region is only covered by SiC channels, therefore the HeII $\lambda 1084.9$ line was given a small weight in the analysis.

The resulting combined spectra, normalized to the local continuum, are shown in Figure 1. These plots also show a model of interstellar atomic and molecular hydrogen calculated for the line of sight of each star (see BG02 and GB04 for details) using $E(B - V)$ values 0.92, 0.71 and 0.80 for HD 16691, HD 151300 and HD 152386, taken from the literature. These $H_2 + HI$ calculated absorption spectra are useful to assess which observed features are purely stellar and to determine reliable continuum regions for flux normalization. Interstellar H_2 and HI absorption is severe in the FUSE wavelength range.

2.2. UV spectra

IUE observations (1200-3200Å) exist for HD 152386 (low resolution, $\Delta\lambda \approx$ 6Å) and HD 16691 (at resolution of both $\Delta\lambda \approx 0.2$Å and 6Å). With the tools in the MAST database, we examined all the observations of both targets taken with the SWP camera (1150-1975Å), to check for variability and to exclude saturated portions, and chose the data with the best S/N. We discarded the high resolution spectrum of HD 16691 because some portions have negative flux. We then downloaded the selected spectra from the INES

archive (Wamsteker et al., 2000) because the data typically have a better background correction at wavelengths shorter than 1400Å, where overlap between echelle orders is significant (Bianchi & Bohlin 1984). HD 151300 has not been observed in this spectral range. The normalized IUE spectra in the wavelength range containing the strongest spectral lines (1200-1750Å) are shown in Figure 2. Table 1 compiles the FUSE and IUE datasets used in this work.

3. Spectral line morphology

In Figures 1 and 2 we compare the FUSE (1010-1180Å portion) and IUE (1200-1750Å) spectra of HD 16691 and HD 152386 with the spectra of supergiant stars analysed by BG02 and GB04. The combined sample covers spectral types O4 to O7, and line variations across this range can be examined.

Figure 1 shows that the strength of OVI $\lambda\lambda$1031.9,1037.6 is approximately constant through spectral types O4-O7. SIV $\lambda\lambda$1062.7,1073.0,1073.5 display strong P Cygni profiles in HD 152386 (the emission of the bluest component being masked by hydrogen absorption) as in the other mid-O supergiants; these lines have maximum strength around type O6 and weaken towards both earlier and later types.

The PV $\lambda\lambda$1118.0,1128.0 + SiIV $\lambda\lambda$1122.5,1128.3,1128.4 blend has similarly maximum strength around type O6 but smaller variation across these types. Its profile changes, with the absorption being deeper on the shorter wavelength side at earlier spectral types, suggesting that these lines are formed in different layers of the wind (Bianchi et al., 2000). They are also known to be sensitive to wind clumping. The strength of the CIVλ1169 + CIIIλ1176 lines, which we found in BG02 and GB04 to be a temperature indicator for stars of similar luminosity class, decreases from the O7 to the O4 supergiants.

The present sample includes two O6 supergiants, HD 210839 and HD 152386. The lines in the FUSE spectra of HD 210839 are generally weaker than in the other O6-O7 supergiants, as pointed out by BG02. The line strength in the spectrum of HD 152386 follows better the smooth trend of variations with spectral type observed across the sample, although HD 210839 has the same luminosity class based on its optical spectra.

The most prominent features in the IUE range (Figure 2) are SiIV $\lambda\lambda$1393.8, 1402.8, NV $\lambda\lambda$1238.8,1242.8 and CIV $\lambda\lambda$1548.2,1550.8 which show fully de-

veloped P Cygni profiles in all the supergiants. SiIV $\lambda\lambda$1393.8,1402.8 follows the behaviour of CIVλ1169 + CIIIλ1176 and decreases towards earlier types. The emission of CIV $\lambda\lambda$1548.2,1550.8 is stronger in the early type supergiants and HD 210839. NV $\lambda\lambda$1238.8,1242.8 does not exhibit a clear trend, in this range.

The OIV $\lambda\lambda$1339,1343 and OV λ1371 absortions, and the NIV λ1718 P Cygni profile, grow stronger towards the earlier types. The spectra of HD 190429A and HD 16691 (both O4 If$^+$) display HeII λ1640.0 emission, characteristic of O3-O5 If stars (Walborn, Nichols-Bohlin, & Panek, 1985; Walborn & Nichols-Bohlin, 1987), that indicates high mass-loss rate (see GB04). The spectra of the O4 supergiants are very similar to each other, but NIV λ1718, SiIV $\lambda\lambda$1393.8,1402.8, CIV $\lambda\lambda$1548.2,1550.8 and PV $\lambda\lambda$1118.0, 1128.0 + SiIV $\lambda\lambda$1122.5,1128.3,1128.4 are stronger in HD 16691. This can be explained by a higher mass-loss rate for this star or, as shown in Section 4.3, a lower effective temperature.

In Figure 1 (top) the FUSE spectrum of HD 151300 is compared with other mid-O type giants studied in BG02. All spectral features exhibit weaker profiles than the supergiants in the same figure, except for OVI $\lambda\lambda$1031.9,1037.6 that has similar strength. The most remarkable case is SIV $\lambda\lambda$1062.7,1073.0,1073.5, with almost no wind profile. Although the comparison covers a smaller spectral range, both PV $\lambda\lambda$1118.0,1128.0 + SiIV $\lambda\lambda$1122.5,1128.3,1128.4 and CIVλ1169 + CIIIλ1176 show variations similar to those seen in supergiants.

4. Analysis of the UV Spectra with Model Atmospheres

We analyzed the far-UV – UV spectra of the program stars, using synthetic atmosphere models computed with the WM-basic code (Pauldrach, Hoffmann, & Lennon, 2001). WM-basic applies a consistent non-LTE treatment of line-blocking to the entire atmosphere and solves the hydrodynamical structure of the spherically expanding envelope, with a smooth transition from the quasi-static photosphere to the high velocity outflow. Soft-X rays produced by shocks in the wind, which affect the ionization of most stages observed in UV, are also taken into account. This parameter can be constrained thanks to the OVI $\lambda\lambda$1031.9,1037.6 doublet in the FUSE range. The best-fitting models obtained from this analysis are shown in Figures 3 and 4, and the derived stellar parameters are listed in Table 2. Below we discuss the analysis of the individual stars.
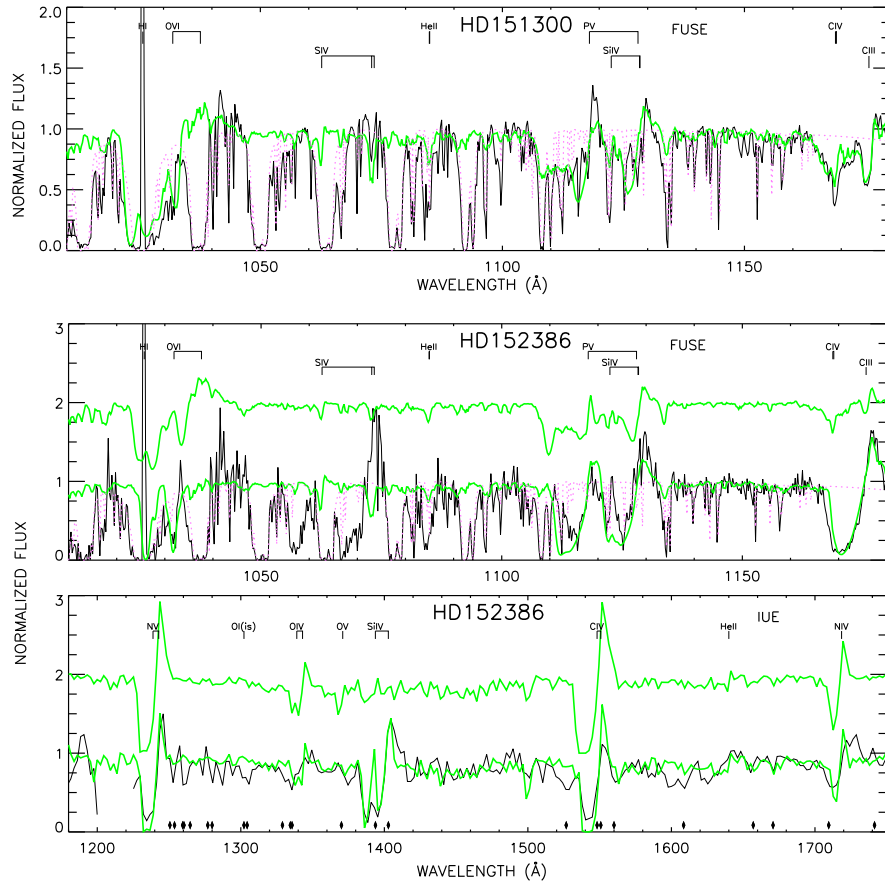
8

Figure 3: **Top:** FUSE spectrum (black) and best fit WM-basic model (green/light grey) of HD 151300. Interstellar hydrogen absorptions (estimated from the reddening value) are shown with a pink/grey-dotted line. The model parameters are given in Table 2. **Bottom:** HD 152386 FUSE (top plot) and IUE (bottom plot) spectra. The positions of the major interstellar lines in the IUE range are indicated with diamonds at the bottom.

9

4.1. HD 151300

The terminal velocity, $v_\infty \simeq 2700$ km s^{-1}, was estimated from v$_{edge}$, measured at the short-wavelength edge of the OVI $\lambda\lambda$1031.9,1037.6 absorption, reduced by 20% to account for turbulence (Groenewegen, Lamers, & Pauldrach, 1989). We computed a small grid of WM-basic models with this terminal velocity, log g =3.6 and $R_* = 16 R_\odot$ (typical for giant stars). $\dot{M}$, log$L_x/L_\odot$ and $T_{\rm eff}$ were constrained from PV $\lambda\lambda$1118.0, 1128.0 + SiIV $\lambda\lambda$1122.5, 1128.3, 1128.4 and CIVλ1169 + CIIIλ1176, whose strength increases by increasing $\dot{M}$ and decreasing log$L_x/L_\odot$ and $T_{\rm eff}$, in this regime, and OVI $\lambda\lambda$1031.9,1037.6 which has the opposite dependence on these parameters.

The lower limit of $T_{\rm eff}$ is 32,000 K, below which CIVλ1169 + CIIIλ1176 displays a saturated absorption in the models, in contrast with the observed spectrum, for the high $\dot{M}$ needed to fit PV $\lambda\lambda$1118.0,1128.0 + SiIV $\lambda\lambda$1122.5,1128.3,1128.4. This behaviour is observed for the log$L_x/L_\odot$-range where OVI $\lambda\lambda$1031.9,1037.6 is produced (log$L_x/L_\odot \geq$-7.5). The upper limit for $T_{\rm eff}$ is 38,000 K, when PV $\lambda\lambda$1118.0,1128.0+SiIV $\lambda\lambda$1122.5,1128.3,1128.4 in the models become stronger than observed for the high mass-loss rates needed to produce any CIVλ1169+CIIIλ1176.

The best-fit model has $T_{\rm eff}$ =35,500 K and is shown in Figure 3. The value of log$L_x/L_\odot$ was determined by fitting OVI $\lambda\lambda$1031.9,1037.6. The upper/lower limits for $\dot{M}$ where set to the values that produced PV $\lambda\lambda$1118.0,1128.0 + SiIV $\lambda\lambda$1122.5,1128.3,1128.4 and CIVλ1169 + CIIIλ1176 in excess/defect in the models. We also varied log g and R_* until the resulting model did not fit the observations, yielding the error bars for these parameters.

4.2. HD 152386

The terminal velocity was determined from v$_{\rm edge}$ measurements of all the spectral transitions showing a wind profile. However, none of these lines is saturated, except for OVI $\lambda\lambda$1031.9,1037.6 which is not useful since the bluest part of its absorption overlaps with an H$_2$ transition (Figure 1). Therefore we can only obtain a lower limit of $v_\infty \gtrsim$1800km s^{-1}.

Our extensive grid of WM-basic models for supergiant stars (log g =3.4, $R_* = 21 R_\odot$) indicates that $\dot{M} \geq 1 \cdot 10^{-6}$ M$_\odot$ yr^{-1} is required to match the observed P Cygni of CIIIλ1176. In this regime of $\dot{M}$, $T_{\rm eff}$ is constrained with PV $\lambda\lambda$1118.0,1128.0 + SiIV $\lambda\lambda$1122.5,1128.3,1128.4, CIVλ1169 + CIIIλ1176 and SiIV $\lambda\lambda$1393.8,1402.8 (the three having the same dependence on $T_{\rm eff}$, $\dot{M}$ and log$L_x/L_\odot$). NIV λ1718, which increases with increasing $T_{\rm eff}$ and

$\dot{M}$ but is not sensitive to $\log L_x/L_\odot$, provides a further constraint. The lower limit is $T_{\rm eff}$ =32,000 K. Models with lower temperatures and the high mass-loss rates needed to match CIVλ1169 + CIIIλ1176 absorption, have stronger than observed PV $\lambda\lambda$1118.0,1128.0 + SiIV $\lambda\lambda$1122.5,1128.3,1128.4 and SiIV $\lambda\lambda$1393.8,1402.8, even when extremely high shocks ($\log L_x/L_\odot$=-6.3) are assumed. In these models, the emission of CIVλ1169+CIIIλ1176 is not as strong as observed and NIV λ1718 is too weak. The upper limit of the effective temperature is 36,000 K. Above this value CIVλ1169 + CIIIλ1176 does not develop a P Cygni profile and SiIV $\lambda\lambda$1393.8,1402.8 is absent, according to our models, even at high mass-loss rates that lead to too strong PV $\lambda\lambda$1118.0,1128.0 + SiIV $\lambda\lambda$1122.5,1128.3,1128.4. lines in the model spectra.

$\dot{M}$ and $\log L_x/L_\odot$ were constrained from the model that provides the best overall fit to OVI $\lambda\lambda$1031.9,1037.6, PV $\lambda\lambda$1118.0,1128.0 + SiIV $\lambda\lambda$1122.5,1128.3,1128.4, CIVλ1169+CIIIλ1176, SiIV $\lambda\lambda$1393.8,1402.8 and NIV λ1718. We then varied $\log g$ and R_* to find the acceptable range of values for these parameters, although they can only be loosely constrained from wind lines. The best fit model is shown in Figure 3.

Models with high mass-loss rates, as required to fit the CIIIλ1176 lines, do not match the observed OVI $\lambda\lambda$1031.9,1037.6 emission in the $T_{\rm eff}$ =32,000-36,000 K range. Higher $T_{\rm eff}$'s are needed to fit this doublet: in Figure 3. 4 we compare the best-fit model with one having similar parameters but $T_{\rm eff}$ =38,000 K. The higher $T_{\rm eff}$ model matches the OVI $\lambda\lambda$1031.9,1037.6 profile, but PV $\lambda\lambda$1118.0,1128.0 + SiIV $\lambda\lambda$1122.5,1128.3,1128.4, CIVλ1169+CIIIλ1176 and SiIV $\lambda\lambda$1393.8,1402.8 are fainter, and NIV λ1718 and OIV $\lambda\lambda$1339,1343 stronger than in the observed spectrum, indicating that $T_{\rm eff}$=38,000 K is too high. The 34,000 K model does fit the absorption at $\lambda \sim$1032Å, which is the blue-shifted red component of the doublet. This analysis indicates that a different treatement of shocks in the winds and inclusion of clumping is needed (e.g. BHG09), which we plan as a continuation of this program with the CMFGEN code .

The best-fit model fails to match the strong SIV $\lambda\lambda$1062.7,1073.0,1073.5 profiles and the unsaturated absorption of NV $\lambda\lambda$1238.8,1242. These problems, also encountered in BG02 and GB04, probably originate in the sulfur model used by WM-basic and the treatment of shocks. There is also a mismatch between the model and observed CIV $\lambda\lambda$1548.2,1550.8 lines. While it is possible to fit their profile with models of sub-solar carbon abundance ($X_C = 0.01\ X_{C,\odot}$), such models cannot match the observed CIVλ1169 +

CIIIλ1176. HD 152386 is a binary (detected only with speckle interferometry, Mason et al. 1998) but this fact alone cannot account for the discrepancy, since a possible contribution by the companion would also affect other spectral lines.

4.3. HD 16691

The spectra of this star and our analysis to constrain its parameters are rather similar to HD 190429A, analyzed by GB04. However, no consistent fit of all line diagnostics could be obtained using models with solar abundances. The best-fit model with solar abundances is shown in Figure 4, upper panel. In this model, the strength of OVI $\lambda\lambda$1031.9,1037.6, CIV $\lambda\lambda$1548.2,1550.8 and HeII λ1640.0 are discrepant with the observations. A much better match is obtained by using CNO abundances for a slightly evolved star $X_{He} = 5\ X_{He,\odot}$, $X_C = 0.5\ X_{C,\odot}$, $X_N = 2.0\ X_{N,\odot}$, $X_O = 0.1\ X_{O,\odot}$ (lower panel in Figure 5). The analysis thus indicates that this star may be evolved. The stellar parameters (given for both fits in Table 2) do not differ significantly among the models with different abundances, therefore the abundance uncertainty does not influence our T_{eff} calibration. Bouret et al. (2012) also analyzed this star, using the CMFGEN code, and found a slightly higher T_{eff} (40,000K, *vs* our result of $T_{\text{eff}} = 37,000 \pm 2,000$K), but otherwise very similar parameters, and C,O sub-solar, N super-solar abundances, similar to what our analysis with WM-basic indicates.

Table 2: Stellar parameters from model fitting of far-UV and UV spectra.

Star	Sp.Type (ref)	T_{eff} (kK)	log g	R $((R_\odot))$	M $M_\odot$	$L_{bol}/L_\odot$ log	v_∞ (km s^{-1})	$\dot{M}$ 10^{-5} M$_\odot$ yr^{-1}	$L_x/L_\odot$ log
HD 16691[a]	O4 If$^+$(1)	37.0±2.	3.4±.3	25±3	57	6.0±0.2	2100±200	1.0±0.2	-6.75±0.5
		36.5±2.	3.4±0.3	25±3	57	6.0±0.2	2200±200	0.9±0.2	-6.75±0.5
HD 151300	O5.5 III(f)(2)	$35.5^{+2.5}_{-3.5}$	3.7±0.3	16±3	47	5.6±0.3	2700±300	0.2±0.3	-6.5±0.5
HD 152386	O6 Iafpe (1)	34.0±2.	3.3±0.3	21±3	40	5.7±0.2	$\gtrsim$1800	0.4±1.0	-7.0±0.5

References:(1) Walborn (1973), (2) Garrison, Hiltner, & Schild (1977)

a The first line lists the parameters for the best-fit model with solar abundances, the second line for the model with CNO abundances: $X_{He} = 5\ X_{He,\odot}$, $X_C = 0.5\ X_{C,\odot}$, $X_N = 2.0\ X_{N,\odot}$, $X_O = 0.1\ X_{O,\odot}$

5. Discussion

Figure 5 shows the derived T_{eff} 's versus spectral type, combining the samples from this work, BG02, GB04 and BHG09. Our results are compared with past calibrations, based on compilations from plane-parallel, pure H and He analyses (Vacca et al., 1996; de Jager & Nieuwenhuijzen, 1987), and with the calibration by Martins, Schaerer, & Hillier (2005), based on line-blanketed model analysis of optical data. The latter is closer to our results, although a small systematic discrepancy remains. This discrepancy may be resolved by combining more diagnostic lines and with a different treatment to constrain wind clumping, as shown by e.g. BHG09, and by Bouret et al. (2012). We stress that this analysis is solely based on UV lines, independent of constraints from optical lines, that will be included in a future work (as in BHG09). Such analsyis may lead to a further slight revision of stellar parameters, as well as provide insight on the characteristics of wind clumping. Clumping has been discussed e.g. by Puls, Vink & Najarro (2008), Najarro, Hanson, & Puls, J. (2011), see also also Bianchi 2012 and references therein, Herald & Bianchi 2011, Keller et al. 2011, Kaschinski et al. 2012 for discussions on the importance of a consistent modeling, and on the effects on treatement of clumping in UV line analysis in evolved hot stellar objects, where similar issues are at play as those recalled in this work for massive stars, and e.g. Oskinova et al. 2007 for additional discussion. Understanding wind clumping is especially relevant for reconciling UV and optical line diagnostics, ultimately to precisely constrain mass-loss rate, an important parameter to understand massive stars' evolution.

Bianchi, L., & Bohlin, R.C. Quantification of the order overlap problem for IUE high resolution spectra (SWP camera). A correction algorithm. A&A, 134, 31. 1984

Bianchi, L., et al. Measuring the ionization of O star winds. 2000, ApJ, 538, L57

Bianchi, L., & Garcia, M. The Effective Temperatures of mid-O type stars. ApJ, 581, 610. 2002 (*BG02*)

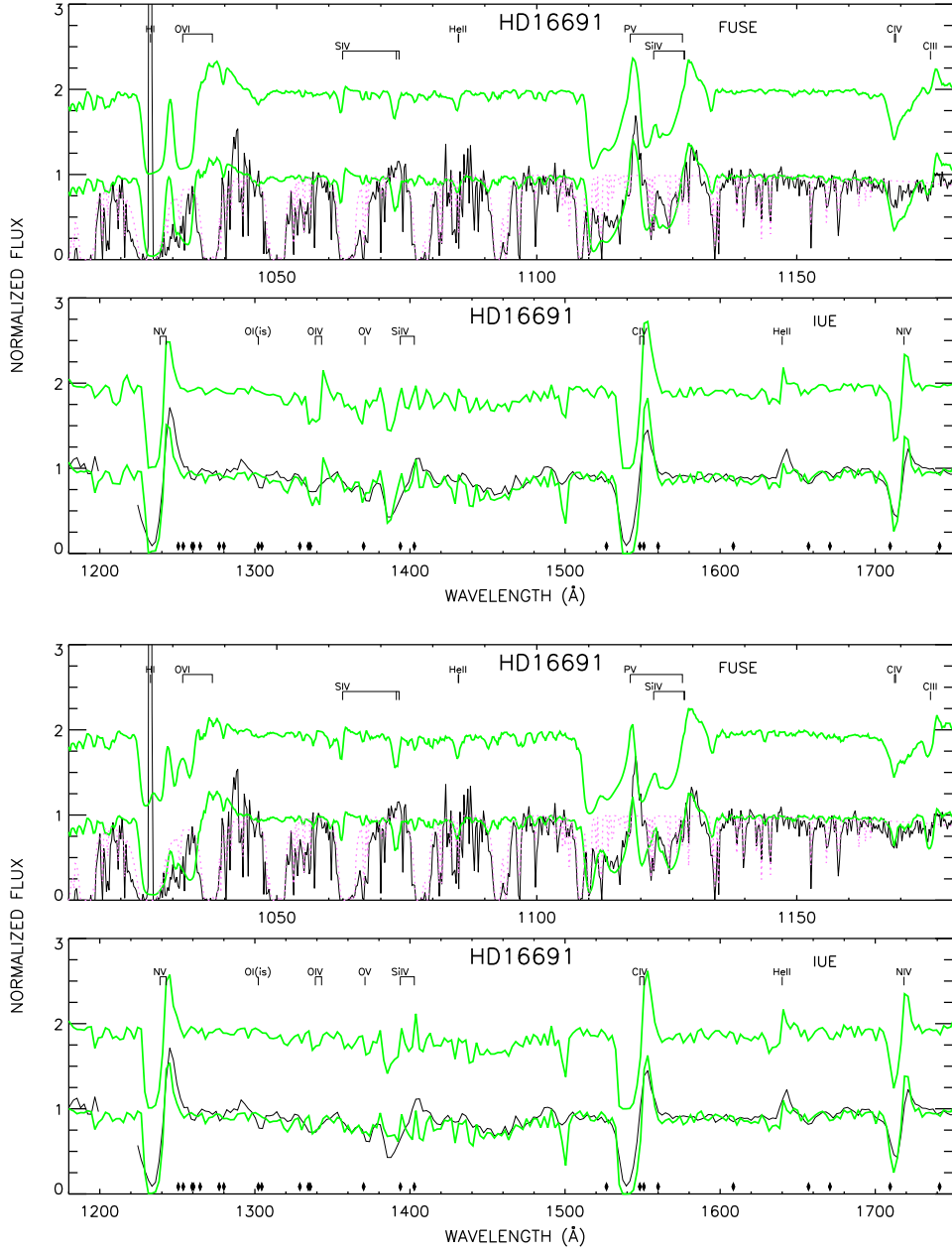Figure 4: HD 16691 spectra and WM-basic models. **Top:** best-fit models with solar abundances. The lower model ($T_{\rm eff}$ =36,000 K, $\dot{M}$=8· $10^{-6} {\rm M}_\odot$ yr^{-1}, log$L_x/L_\odot$=-6.75) fits better lines in the IUE range. However, higher $T_{\rm eff}$ (upper model, $T_{\rm eff}$ =38,000 K, $\dot{M}$=1.2· $10^{-6} {\rm M}_\odot$ yr^{-1}, log$L_x/L_\odot$=-6.75) matches better the emission component of OVI and the HeII line. With the high $\dot{M}$ necessary to produce HeII λ1640 emission in the models ($\dot{M}\geq 7 \cdot 10^{-6} {\rm M}_\odot$ yr^{-1}, GB04), OIV is too strong in any model. This discrepancy can be removed adopting non-solar abundances. **Bottom:** Best-fit models with modified CNO abundances: $X_{He} = 5\ X_{He,\odot}$, $X_C = 0.5\ X_{C,\odot}$, $X_N = 2.0\ X_{N,\odot}$, $X_O = 0.1\ X_{O,\odot}$. The lower model ($T_{\rm eff}$ =37,000 K, $\dot{M}$=8.3· $10^{-6} {\rm M}_\odot$ yr^{-1}, log$L_x/L_\odot$=-6.75) fits better NIV, CIV and PV lines but less well the SiIV lines. The latter are better matched by a model with a lower $T_{\rm eff}$ (36,000 K) and higher $\dot{M}$=9.6· $10^{-6} {\rm M}_\odot$ yr^{-1}, which, however, provides a worse fit to CIII and PV lines. The lower oxygen abundance improves the fit to OIV.

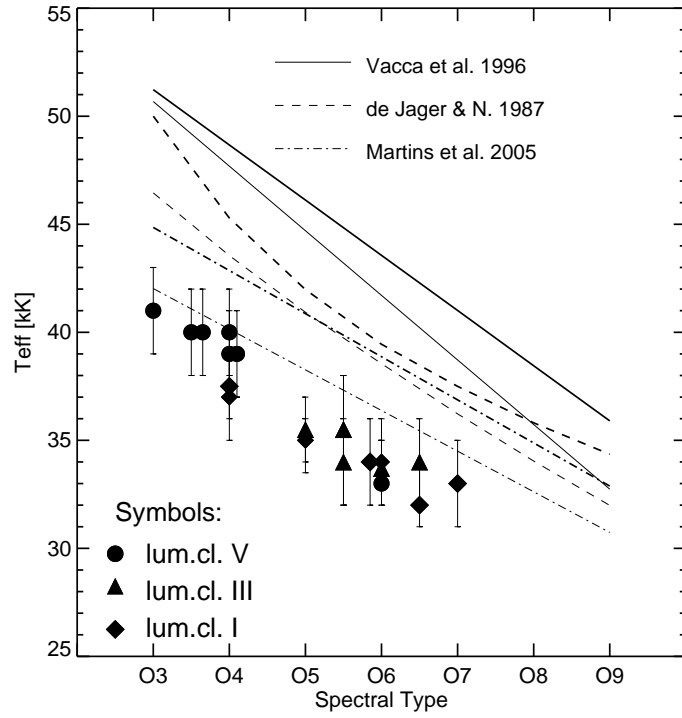Figure 5: T_{eff} versus spectral type for stars from this paper, BG02, BHG09 and GB04. Calibrations of Vacca et al. (1996) (solid line), de Jager & Nieuwenhuijzen (1987) (dashed line) and Martins, Schaerer, & Hillier (2005) (dash-dotted line) are shown, with thick lines for main sequence stars and thin lines for supergiants. Although the sample (with both FUSE and high resolution UV spectra available) is very limited, at spectral type O4 the difference between luminosity class IV and I in our results is similar to that seen in the calibrations by Martins, Schaerer, & Hillier (2005) and de Jager & Nieuwenhuijzen (1987), although our derived temperatures are lower all across the range. For later types the difference among luminsity classes is smaller, and the scatter among the data points is higher.

16

Bianchi, L., Herald, J., & Garcia, M. The fundamental parameters of massive stars. AIPC, 1135, 145. 2009 (*BHG09*)

Bianchi, L. New Advances in the Field of Planetary Nebulae from Ultraviolet Observations. IAU Symp 283, p.45. 2012

Bouret, J.-C., Hillier, J., Lanz, T. Fullerton, A.Properties of Galactic early-type O-supergiants. A combined FUV-UV and optical analysis. A&A. 544, 67. 2012

Garcia, M. & Bianchi, L. The Effective Temperatures of Massive Stars. II. The Early-O types. ApJ, 606, 497. 2004 (*GB04*)

Dixon, V., Kruk, J. & Murphy, E. The CalFUSE Pipeline Reference Guide, available electronically at http://fuse.pha.jhu.edu/analysis/pipeline_reference.html. 2001

Garrison, R. F., Hiltner, W. A., & Schild, R. E. MK spectral classifications for southern OB stars. ApJS, 35, 111. 1977

de Jager, C., & Nieuwenhuijzen, H.A new determination of the statistical relations between stellar spectral and luminosity classes and stellar effective temperature and luminosity. A&A, 177, 217. 1987

Groenewegen, M. A. T., Lamers, H. J. G. L. M., & Pauldrach, A. W. A. The winds of O-stars. II - The terminal velocities of stellar winds of O-type stars. A&A, 221, 78. 1989

Herald, J., & Bianchi, L. The Winds of Hydrogen-Rich Central Stars of Planetary Nebulae. MNRAS, 416, 2440. 2011

Puls, J. Vink, J. & Najarro, F. Mass loss from hot massive stars.Astronomy and Astrophysics Review, 16, 209. 2008

Herrero, A., Puls, J., & Najarro, F. Fundamental parameters of Galactic luminous OB stars VI. Temperatures, masses and WLR of Cyg OB2 supergiants. A&A, 396, 949. 2002

Hillier, D. J. & Miller, D. L. The Treatment of Non-LTE Line Blanketing in Spherically Expanding Outflows. ApJ, 496, 407. 1998

Hillier, D. J., & Miller, D. L. Constraints on the Evolution of Massive Stars through Spectral Analysis. I. The WC5 Star HD 165763. ApJ, 519, 354. 1999

Kaschinski, C.B., Pauldrach, A.W.A., and Hoffmann, T.L. Radiation-driven winds of hot luminous stars. XVII. Parameters of selected central stars of PN from consistent optical and UV spectral analysis and the universality of the mass-luminosity relation. A&A, 542, 45. 2012

Keller, G., et al. 2011, A Grid of Synthetic Models for the Analysis of [WC] CSPNe. MNRAS, 418, 705. 2011

Lindler, D. available electronically at: http://fuse.pha.jhu.edu/analysis/fuse_idl_tools. 2002

Martins, F., Schaerer, D., & Hillier, D. J. 2005, A new calibration of stellar parameters of Galactic O stars. A&A, 436, 1049. 2005

Mason, B. D., Gies, D. R., Hartkopf, W. I., Bagnuolo, W. G., Jr., ten Brummelaar, T., & McAlister, H. A. 1998, AJ, 115, 821

Najarro, F.; Hanson, M. M.; Puls, J. L-band spectroscopy of Galactic OB-stars. A&A, 535, 32. 2011

Oskinova, L. et al. Neglecting the porosity of hot-star winds can lead to underestimating mass-loss rates. A&A, 476, 1331. 2007

Pauldrach, A.W.A., Hoffmann, T. L. & Lennon, M. Radiation-driven winds of hot luminous stars. XIII. A description of NLTE line blocking and blanketing towards realistic models for expanding atmospheres. A&A, 375, 161. 2001

Puls, J., Urbaneja, M. A., Venero, R., Repolust, T., Springmann, U., Jokuthy, A., & Mokiem, M. R. Atmospheric NLTE-models for the spectroscopic analysis of blue stars with winds. II. Line-blanketed models. A&A, 435, 669. 2004

Repolust, T., Puls, J., & Herrero, A. Stellar and wind parameters of Galactic O-stars. The influence of line-blocking/blanketing. A&A, 415, 349. 2004

Sahnow, D., Moos, H. W., Ake, T. B. et al. On-Orbit Performance of the Far Ultraviolet Spectroscopic Explorer Satellite. ApJ, 538, L7. 2000

Sahnow, D. The FUSE Instrument and Data Handbook. available only electronically at http://fuse.pha.jhu.edu/analysis/IDH/IDH.html .2002

Vacca, W. D., Garmany, C. D., & Shull, J. M. The Lyman-Continuum Fluxes and Stellar Parameters of O and Early B-Type Stars. ApJ, 460, 914. 1996

Walborn, N. R. The space distribution of the O stars in the solar neighborhood. AJ, 78, 1067. 1973

Walborn, N. R., & Nichols-Bohlin, J. Ultraviolet spectral morphology of the O stars. IV - The OB supergiant sequence. PASP, 99, 40. 1987

Walborn, N. R., Nichols-Bohlin, J., & Panek, R. J. International Ultraviolet Explorer Atlas of O-Type Spectra from 1200 to 1900 Å, NASA RP-1155 (Washington: NASA).1985

Wamsteker, W., Skillen, I., Ponz, J. D., de la Fuente, A., Barylak, M., & Yurrita, I. INES: Astronomy Data Distribution for the Future. Ap&SS, 273, 155. 2000